Journal of Applied Mechanics and Technical Physics, Vol. 47, No. 5, pp. 688–695, 2006

NUMERICAL MODELING OF THERMOPHYSICAL PROCESSES IN LASER-BEAM WELDING WITH FORMATION OF A VAPOR CHANNEL

A. N. Cherepanov, V. P. Shapeev, V. M. Fomin, and L. G. Semin

UDC 621.9.048.7:621.375.826

A quasi-two-dimensional mathematical model of laser welding of plates made of a binary alloy with allowance for metal vaporization and formation of a vapor channel is developed. A difference algorithm and a computer code are designed on the basis of this model. Processes of melting, vaporization, and solidification of the alloy of butt-welded aluminum plates are considered numerically as an example. The shape and depth of the vapor channel and welding bath are calculated for given conditions of the radiation power and welding velocity. Based on semi-empirical relations and numerical data obtained, the characteristic size of the dendritic structure of the solidified melt is estimated.

Key words: *modeling, laser welding, heat transfer, vaporization, vapor channel, two-phase zone, dendritic structure.*

Introduction. Industrial-scale development of the laser-welding technology makes process engineers seek for improvement of the weld-joint quality by creating conditions that ensure formation of a finely disperse defect-free crystal structure, retaining of the initial chemical composition of the joint, and reduction of thermal stresses responsible for origination of cracks inside the welding seam and article deformation. The wide variety of physicochemical and thermohydrodynamic processes proceeding at high velocities and temperatures hinders their experimental investigation and development of rational welding regimes. In this case, the most efficient tools are mathematical modeling and numerical experiments, which, in turn, require adequate mathematical models.

Currently available numerical models take into account only some individual aspects of the sophisticated processes in the welding bath and in the vicinity of the welding seam without analyzing the mutual influence of these factors [1–6]. The issues that have not been adequately studied include structure and phase formation, formation of chemical inhomogeneity in crystallization of multispecies alloys, vaporization of alloying agents in the case of vapor-channel formation, origination of shrinkage porosity, etc.

A mathematical model of thermophysical processes in the welding bath with allowance for vapor-channel formation is formulated in the present paper. Melting and crystallization of a binary aluminum alloy are described under the assumption of quasi-equilibrium in the two-phase zone [7]. Based on the model proposed, the problem is solved numerically in a quasi-two-dimensional approximation. The characteristic size of the dendritic structure and the width of the two-phase zone in the region of crystallization are estimated.

1. Formulation of the Problem. We consider a steady process of laser butt-welding of two plates made of an aluminum alloy. As the thermo- and hydrodynamic processes in the welding region are rather complicated and have not been studied in detail, we apply some simplifying assumptions to the thermophysical problem at this stage. We assume that the laser-beam (welding) velocity is constant, the temperature field and the positions of the phase boundaries in the welding bath are quasi-steady, and the vapor–gas channel is in dynamic equilibrium with the ambient liquid [2, 6]. In the numerical solution of the quasi-two-dimensional equation of heat transfer in the

Khristianovich Institute of Theoretical and Applied Mechanics, Siberian Division, Russian Academy of Sciences, Novosibirsk 630090; ancher@itam.nsc.ru. Translated from Prikladnaya Mekhanika i Tekhnicheskaya Fizika, Vol. 47, No. 5, pp. 88–96, September–October, 2006. Original article submitted July 15, 2005; revision submitted November 7, 2005.

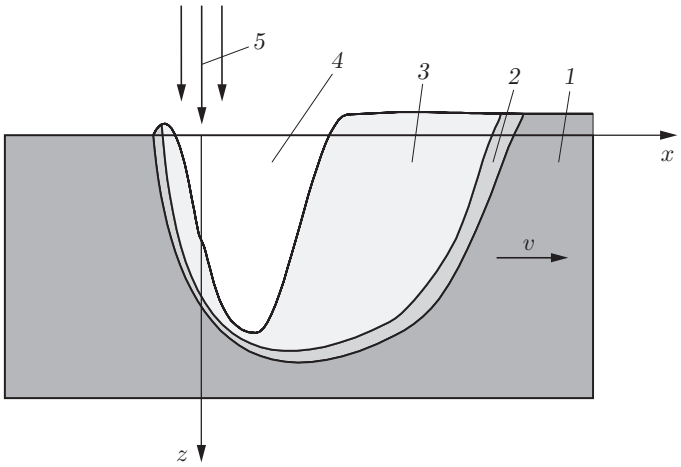

Fig. 1. Layout of the welding bath (section $y = 0$): 1) solid phase; 2) two-phase zone; 3) liquid phase; 4) vapor–gas channel; 5) laser-beam axis.

liquid phase, the convective heat transfer caused by heat transfer from the melting region (from the frontal wall of the channel) to the region of solidification (to the rear wall) [3, 6] is modeled by introducing an effective source of heat into the equation of thermal balance on the surface of the rear wall of the vapor–gas channel. The vapor is considered as a transparent medium. The effects of optical breakdown and vapor ionization are ignored.

In the domain considered, we introduce a Cartesian coordinate system in which the laser beam incident onto a dense joint of the welded plates is motionless, and the plates move with the welding velocity v. The downward z direction is coaxial with the beam, the x axis is directed along the joint and follows the direction of motion of the plates, and the y axis is perpendicular to the joint. The origin lies at the beam axis on the upper surfaces of the plates (Fig. 1). To protect the metal from oxidation, the welded plates are subjected to a neutral gas flow, which partly entrains metal vapors.

2. Governing Equations and Relations. In the chosen coordinate system, the quasi-steady equations of heat transfer can be written in the form

$$c_{ei} v \frac{\partial T}{\partial x} = \lambda_i \Big(\frac{\partial^2 T}{\partial x^2} + \frac{\partial^2 T}{\partial y^2} + \frac{\partial^2 T}{\partial z^2} \Big); \tag{1}$$

$$c_{ei} = \begin{cases} c_1 \rho_1, & T < T_e, \\ c_2 \rho_2 \Big(1 + \dfrac{\varkappa}{c_2} \dfrac{\partial f_l}{\partial T} \Big), & T_e \leqslant T \leqslant T_{l0}, \\ c_3 \rho_3, & T_{l0} < T, \end{cases} \tag{2}$$

where c_i, λ_i, and ρ_i are the specific heat, thermal conductivity, and density of the ith phase (the subscripts $i = 1$, 2, and 3 refer to parameters of the solid, two-phase, and liquid states of the metal, respectively), T_{l0} and T_e are the temperatures of the beginning and end of metal solidification, f_l is the section (fraction) of the liquid phase in the two-phase zone, and $\varkappa$ is the latent heat of melting.

We consider welding of plates made of the binary alloy Al + 10% Si (by weight). The equation of state of the alloy is approximated by the linear function

$$T_l = T_A - \beta C, \tag{3}$$

where T_l is the liquidus temperature, T_A is the temperature of melting of the pure solvent component, β is the absolute value of the slope of the liquidus line, and C is the concentration of the alloying agent. The relation between the concentration C and the liquid-phase section is described by the Sheil equation [7]

$$C = C_0 f_l^{k-1}, \tag{4}$$

where C_0 is the initial concentration of the alloying agent in the alloy considered and k is the distribution coefficient.

Substituting Eq. (4) into Eq. (3) and taking into account the condition of quasi-equilibrium in the two-phase zone [$T = T_l(C)$], we obtain the relation between f_l and the temperature T:

$$T = T_A - \beta C_0 f_l^{k-1}. \tag{5}$$

Differentiating the left and right sides of Eq. (5) with respect to T, we find the value of $\partial f_l/\partial T$:

$$\frac{\partial f_l}{\partial T} = \frac{1}{\beta C_0 (1-k) f_l^{k-2}}. \tag{6}$$

We assume that welding is performed by radiation of a CO_2 laser with a wavelength $\lambda_0 = 10.6$ μm. The radiation intensity is described by the normal Gaussian distribution

$$I(x, y, z) = I_0 \exp\left(-2(x^2 + y^2)/r_z^2\right),$$

where $I_0 = 2W/(\pi r_z^2)$, W is the laser power, and r_z is the laser-beam radius at a depth z of the vapor–gas channel described by the formula [8]

$$r_z = \sqrt{r_F^2 + \Big(\frac{z - Z_F}{\pi r_F}\,\lambda_0\Big)^2}. \tag{7}$$

Here r_F is the laser-beam radius in the focal plane and Z_F is the position of the focus with respect to the upper surfaces of the welded articles. Then, the expression for the power density of radiation absorbed by a surface element of the vapor–gas channel $z = Z_c(x, y)$ can be written as

$$q(x, y, Z(x, y)) = \frac{2W_{\text{abs}}}{\pi r_z^2}\,\exp\Big(-\frac{2r^2}{r_z^2}\Big), \tag{8}$$

where W_{abs} is the total value of the entire multiply absorbed power and r_z is determined by Eq. (7).

3. Boundary Conditions. According to the assumptions used in formulating the boundary conditions, the losses due to radiation absorption by the vapor–gas cloud partly entrained by the neutral gas are ignored; the gas flow is assumed to be laminar. In this case, the equations on the surface $z = 0$ in regions of the solid, solidified, and liquid alloy and in the two-phase region are

$$\lambda_i \frac{\partial T}{\partial z}\Big|_{z=0} = (\alpha_k + \alpha_{ri})\Big(T\Big|_{z=0} - T_g\Big), \qquad i = 1, 2, 3, \tag{9}$$

where T_{g} is the temperature of the protective gas, $\alpha_{ri} = \varepsilon_i \sigma_0 (T^2|_{z=0} + T_g^2)(T|_{z=0} + T_g)$ is the radiative component of heat transfer (ε_i and σ_0 are the reduced emissivity and the Stefan–Boltzmann constant, respectively), α_k is the coefficient of convective heat transfer determined in the form [9]

$$\alpha_k = 0.646\,\text{Re}^{1/2}\,\text{Pr}^{\,1/3}\lambda_g/l; \tag{10}$$

$\text{Re} = v_g l/\nu_g$, $\text{Pr} = \nu_g/a_g$, v_{g} is the gas-flow velocity, l is the characteristic length of the cooling zone, and ν_{g}, a_{g}, and λ_{g} are the kinematic viscosity, thermal diffusivity, and thermal conductivity of the gas, respectively. A condition similar to Eq. (9) is also valid on the lower surfaces of the welded plates at $z = h$.

The zone of laser radiation [on the surface of the vapor channel $z = Z_c(x, y)$] obey the equation

$$-\lambda_3 \nabla T \cdot \boldsymbol{n} = \boldsymbol{q} \cdot \boldsymbol{n} - L\dot{m} + \delta q_c, \tag{11}$$

where $\dot{m}$ is the mass rate of matter vaporization from a unit surface, which is related to the excess vapor pressure $P(z)$ necessary to prevent the channel wall from collapsing by the expression $\dot{m} = \sqrt{P(z)\rho_v}$, ρ_v is the vapor density, L is the specific heat of vaporization of the alloy, $\boldsymbol{q}$ is the absorbed flux of radiation with allowance for secondary reflections, $\delta = 0$ on the frontal wall of the channel and $\delta = 1$ on the rear wall, and q_c is the convective heat flux transferred from the frontal to the rear wall of the channel, which is determined by the relation $q_c = c_3\rho_3 v_r(T_1 - T)$, where T_1 is the averaged value of temperature on the frontal wall of the channel, and v_r is the mean velocity of the melt in the channel, whose value was estimated in accordance with [6, 10]. In determining the value of W_{abs} in Eq. (8), we assume that the power remaining after the first reflection [$W_1 = (1 - A)W$, where A is the absorption coefficient] is uniformly scattered over the channel surface including the input orifice. In this case, with allowance for secondary reflections, the power absorbed by the channel walls can be approximately calculated via the effective absorption coefficient $A_{\text{eff}} = A + A_e(1 - A)$ by the formula

$$W_{\text{abs}} = A_{\text{eff}} W, \tag{12}$$

where A_e is the equivalent absorption coefficient for multiply reflected laser radiation. Following [3], we find it by the formula

$$A_e = A \sum_{n=1}^{\infty} \Big(\frac{(1-A) S_b}{S_b + S_c} \Big)^n, \tag{13}$$

where S_b and S_c are the areas of the side surface of the channel and the input orifice, respectively. The boundary between the liquid phase and the two-phase zone is determined by the liquidus isotherm

$$T\Big|_{z=\xi_l(x,y)} = T_{l0}, \tag{14}$$

and the boundary between the two-phase zone and the solid (initial or solidified) phase is determined by the isotherm corresponding to the eutectic temperature of the alloy considered:

$$T\Big|_{z=\xi_e(x,y)} = T_e. \tag{15}$$

The phase-transition boundaries should satisfy the condition of temperature continuity and thermal balance.

To simplify the numerical algorithm, we first consider a quasi-two-dimensional model of heat transfer. For this purpose, we average Eq. (1) with respect to the y coordinate to obtain the relation

$$c_{ei} v \frac{\partial T}{\partial x} = \lambda_i \Big(\frac{\partial^2 T}{\partial x^2} + \frac{\partial^2 T}{\partial z^2} \Big) - \frac{\lambda_i}{l_T^2} (T - T_a), \tag{16}$$

where $l_T = 2\sqrt{a_i \tau}$ is the length of propagation of the heat wave during the time $\tau = 2r_F/v$, a_i is the thermal diffusivity of the ith medium, and T_a is the characteristic temperature of the plate outside the averaging domain.

4. Model of Vapor-Channel Formation. In describing laser welding of alloys with rather high radiation powers, an important and difficult problem is modeling of vapor-channel formation under the action of excess pressure of metal vapors, including the response pressure (recoil pressure) balancing the capillary force and the hydrostatic pressure of the melt. In the first approximation, we can determine the shape of this channel by the isotherm T_{sat} of melt boiling under standard pressure:

$$T\Big|_{z=Z_c} = T_{\text{sat}}. \tag{17}$$

The channel boundaries are refined by the conditions of thermal balance (12) and equilibrium of pressure on the channel walls:

$$P(z) = -\sigma K_c + g\rho_3 z, \qquad z = Z_c. \tag{18}$$

Here σ is the surface tension of the alloy, K_c is the curvature of the surface Z_c, and $P(z)$ is the excess vapor pressure, which is the sum of the static pressure during surface vaporization $P_s(z)$ and the recoil (response) pressure $P_r(z)$:

$$P = P_s + P_r. \tag{19}$$

The value of K_c is determined by the relation

$$K_c = \operatorname{div} \Big(\frac{\nabla Z_c}{\sqrt{1 + |\nabla Z_c|^2}} \Big). \tag{20}$$

We write the expression for the saturated vapor pressure in the case of surface vaporization of the jth substance in the alloy [7]:

$$P_{sj} = P_{0j} T^{-1} \exp\left(A_j - B_j/T\right) \tag{21}$$

(P_{0j}, A_j, and B_j are empirical constants). The saturation pressure of the mixture of vaporized components of the alloy is determined by the formula

$$P_s = \sum_{j=0}^{1} 0.01 C_j P_{sj}, \tag{22}$$

where C_j is the molar concentration of the jth component of the alloy ($j = 0, 1$). According to [10], we assume that P_r linearly depends on the pressure P_s: $P_r = bP_s$. Assuming further that the vapor is an ideal gas, which obeys the Clapeyron–Mendeleev equation, we obtain the expressions

$$\rho_j = \frac{\mu_j}{RT^2} \exp\Big(A_j - \frac{B_j}{T}\Big) \tag{23}$$

for the density of the vapor of the jth component and

$$\rho_v = \sum_{j=0}^{1} 0.01 C_j \frac{\mu_j}{RT^2} \exp\Big(A_j - \frac{B_j}{T}\Big) \tag{24}$$

for the mixture (μ_j is the molar weight).

The greatest excess pressure is reached at the channel bottom:

$$P_{\max} = \sigma / r_c + \rho_3 g Z_{c,\max} \tag{25}$$

(r_c is the radius of curvature of the bottom, which is determined by the semi-circumference approximating the surface $z = Z_c$ at the point of the maximum depth of the channel $Z_{c,\max}$). The free upper boundary of the liquid bath $z = Z_w(x, y)$ relates the surface of the vapor channel Z_c with the liquidus Z_l. The equilibrium of the surface Z_w is described by an equation similar to Eq. (18):

$$P = -\sigma \operatorname{div}\Big(\frac{\nabla Z_w}{\sqrt{1 + (\nabla Z_w)^2}}\Big) - \rho_3 g Z_w + B. \tag{26}$$

Here B is a constant characterizing the field of intrinsic stresses, which is determined together with the constants of integration of Eq. (26) from the following boundary conditions:

— in the region of melting and vaporization ($x < 0$),

$$Z_w\Big|_{x=x_c^-} = Z_c\Big|_{x=x_c^-} = 0, \qquad Z_c'\Big|_{x=x_c^-} = Z_w'\Big|_{x=x_c^-}, \qquad Z_w\Big|_{x=x_e^-} = 0; \tag{27}$$

— in the region of vaporization and crystallization ($x > 0$),

$$Z_w\Big|_{x=x_c^+} = Z_c\Big|_{x=x_c^+} = 0, \qquad Z_w'\Big|_{x=x_c^+} = Z_c'\Big|_{x=x_e^+}, \qquad Z_w'\Big|_{x=x_e^+} = 0. \tag{28}$$

Here x_c^- and x_c^+ are the coordinates of the points of intersection of the channel boundaries with the surface $z = 0$; x_e^- and x_e^+ are the coordinates of the points of intersection of the melting-region boundaries with the surface $z = 0$ and of the solidification-region boundary with the weld bed, respectively; the superscripts minus and plus refer to the left and right boundaries with respect to the z axis, respectively.

Equations (16), (18), and (26) with allowance for relations (2), (6), (9)–(15), (17), (19)–(25), (27), and (28) were solved numerically by the finite-difference method.

5. Brief Description of the Numerical Algorithm. In the plane of the section of the welding region considered (see Fig. 1), we choose a computational domain G, whose form at the first stage of the computations (without the vapor channel and the weld bed from the solidified metal) is a rectangle with the sides $z = 0$, $z = h$, $x = -l_1$, and $x = l_2$, where l_1 and l_2 are the distances from the left and right boundaries of the rectangle to the laser-beam axis, respectively. The choice of l_1 and l_2 depends on the laser power and welding velocity.

To solve Eq. (16) numerically on a rectangular difference grid G_h with the nodes $\{kh_1, mh_2\}$ ($k = 0, 1, \ldots, n_1$ and $m = 0, 1, \ldots, n_2$), we use the scheme of the time-dependent method

$$\frac{T_{k,m}^{n+1} - T_{k,m}^n}{\tau} + v\,\frac{T_{k+1,m}^n - T_{k-1,m}^n}{2h_1}$$

$$= a_i\Big(\frac{T_{k-1,m}^{n+1} - 2T_{k,m}^{n+1} + T_{k+1,m}^{n+1}}{h_1^2} + \frac{T_{k,m-1}^n - 2T_{k,m}^n + T_{k,m+1}^n}{h_2^2}\Big) - \frac{a_i}{l_T^2}\,(T_{k,m}^{n+1} - T_a), \tag{29}$$

where $a_i = \lambda_i / c_{ei}$. The starting point of the index k does not coincide with the starting point of the coordinate x.

Scheme (29), which is implicit in terms of the variable x and explicit in terms of z, is implemented in an iterative manner for each m by marching over the index k along the coordinate axes $x = \text{const}$. In addition to scheme (29), we also used a scheme of conventional approximation; the only difference of the latter scheme is that

the value of $T_{k,m}^{n+1}$ in the second difference derivative with respect to z was taken at the time layer with the index $n+1$ to enhance the diagonal prevalence of the matrix of the system of linear algebraic equations (29) to accelerate the convergence of iterations.

The computational domain contains subdomains with different thermal diffusivities corresponding to the liquid, solid, and two-phase states of the metal. Therefore, all subdomains are cyclically tested at each iteration, and all lines with $x = \text{const}$ are consecutively tested in terms of the index m inside a particular subdomain. The iterations are terminated when the maximum absolute value of the residual of the difference equations becomes smaller than a prescribe value in all nodes of the computational grid.

In the present implementation of the numerical algorithm, the derivatives in the boundary conditions are approximated with the first-order accuracy. As soon as the grid node closest to the channel boundary inside the computational domain (near-boundary nodes) are determined, the conditions at the channel boundary are assumed to be shifted to these points. To determine from which point of the channel boundary the conditions are shifted to a particular near-boundary node (as it is necessary to know the direction of the normal to the boundary at the point considered for writing the conditions in the difference form), we determine the points of intersection of two grid lines $x = \text{const}$ and $z = \text{const}$ passing through this node with the channel boundary. The direction of the normal at the boundary point closest to the grid node considered is assumed to be the direction of the perpendicular from this node to the chord passing through two points found at the boundary. The initial approximations of the channel boundaries (frontal and rear ones) are chosen in the form of single-valued functions $x = x_0(z)$ in the entire interval $0 < z < h_c$ (h_c is the channel depth). In this model, approaching the channel boundaries during the iterative process ($k = 1, 2, \ldots$) follows certain single-valued functions of the form $x = x_k(z)$. If there is no point of intersection of the channel boundary with the grid line $x = \text{const}$ passing through the considered node near the frontal boundary of the channel in the vicinity of the upper boundary of the domain $z = 0$, we have to additionally seek for the point of intersection of the grid line with the tangential line to the frontal boundary of the channel drawn from the point $z = 0$. The derivative with respect to x in the node (x_k, z_m) near the frontal boundary is approximated by the relation $(T_{k,m} - T_{k-1,m})/h_1$, and the derivative with respect to z is approximated by the relation $(T_{k,m} - T_{k,m-1})/h_2$. This allows us to write the conditions on the channel boundary in the difference form. The conditions on the rear wall of the channel are written in a similar manner. To speed up the iterations in the time-dependent method, these conditions are supplemented by a dummy difference derivative of the solution in this near-boundary node with respect to time as an additional term. To implement these conditions into the iterative process (marching along the x axis), the unknowns at each current iteration are taken only in two neighboring nodes in terms of x, whereas the coefficients at these unknowns and the remaining terms are borrowed from the previous iteration. Thus, these conditions are simultaneously linearized with respect to unknowns calculated by marching along a particular grid line $x = \text{const}$.

Similarly, the conditions of thermal balance on the boundaries of subdomains occupied by different phases of the metal are approximated with the first-order accuracy.

The main aspect in the iterative process is the positions of the vapor-channel boundaries. As soon as they are stabilized, the temperature in the vicinity of the vapor channel changes little during further iterations and is almost independent of the changes in temperature at a certain distance from the channel in the computational domain on the side of the rear wall of the channel. Experiments on convergence of the numerical solution with the use of different grids show that the convergence is of the first order or better. The number of nodes in the computations reached $3.5 \cdot 10^6$.

6. Analysis of Numerical Modeling Results. Some results of the numerical computations of butt-welding of two plates made of the AL2 alloy (Al + 10% Si) are presented below. The initial data for the physical quantities of the alloy were taken from [9, 10]: $\lambda_1 = 155.7$ W/(m·K), $\lambda_2 = 127.85$ W/(m·K), $\lambda_3 = 100$ W/(m·K), $c_1 = 1000$ J/(kg·K), $c_2 = 1050$ J/(kg·K), $c_3 = 1100$ J/(kg·K), $\rho_1 = 2.6 \cdot 10^3$ kg/m^3, $\rho_2 = 2.45 \cdot 10^3$ kg/m^3, $\rho_3 = 2.3 \cdot 10^3$ kg/m^3, $T_A = 933$ K, $T_{l0} = 862$ K, $T_l = 850$ K, $\varkappa = 5.37 \times 10^5$ J/kg, $L = 1.11 \cdot 10^7$ J/kg, $C_{10} = 10\%$, $\beta_1 = 7.1$ K/%, $k_1 = 0.14$, $A = 0.65$, $r_F = 10^{-4}$ m, $Z_F = 0$, $T_{\text{g}} = 293$ K, $\lambda_{\text{g}} = 0.024$ W/(m·K), $\nu_{\text{g}} = 1.37 \cdot 10^{-5}$ m^2/sec, $T_{1v} = 2720$ K, $T_{2v} = 2628$ K, $A_1 = 33.294$, $B_1 = 37{,}723.14$ K, $A_2 = 43.584$, $B_2 = 63{,}590.782$ K, $P_{10} = P_{20} = 1$ N/m^2, $\sigma = 0.57$ N/m, $\varepsilon_1 = 0.176$, $\varepsilon_2 = \varepsilon_3 = 0.18$, $v_{\text{g}} = 0.5$ m/sec, $l = 0.1$ m, and $b = 0.55$.

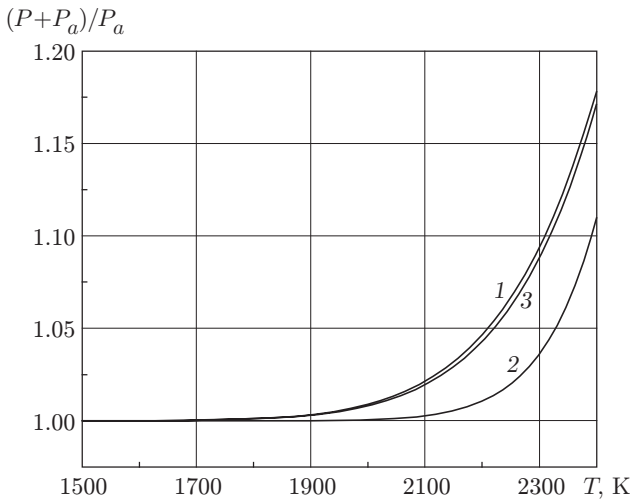

Fig. 2. Partial pressures of the vaporized components of the alloy [aluminum (1) and silicon (2)] and total pressure (3) versus temperature.

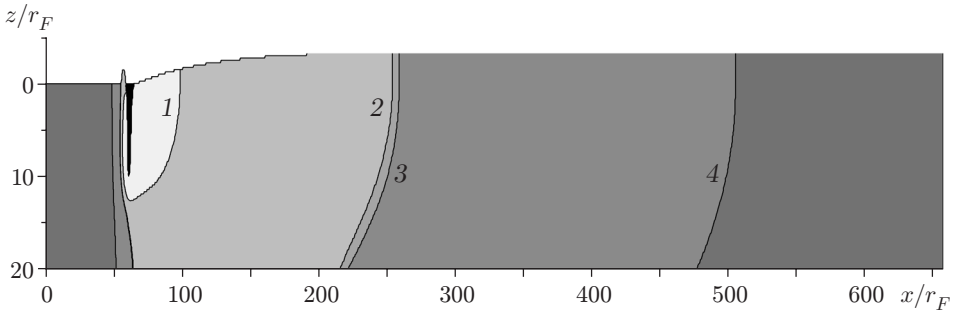

Fig. 3. Temperature field in the computational domain: 1) $T = 1207$ K; 2) $T_{l0} = 862$ K (beginning of solidification); 3) $T_e = 850$ K (end of solidification); 4) $T = 517$ K.

The results computed for the welding velocity $v = 0.08$ m/sec and radiation power $W = 4$ kW are plotted in Figs. 2 and 3.

Figure 2 shows the total and partial pressures of Al and Si vapors as functions of temperature. This dependence describes vaporization of the binary alloy considered with allowance for its chemical composition.

Figure 3 shows the isotherms in the welding bath and the shape of the vapor channel. To have a more clear presentations, we use different scales in the x and z directions, because the length of the computational domain is much greater than its height. Different intervals of temperature variation are indicated by the gray scale (higher values are shown by less intense color). The vapor-channel region has the form of a black cone turned upside down. It follows from the computations that the region with the highest temperature gradients is located in the vicinity of the frontal boundary of the channel (in the melting region). The isothermal surfaces on the right of the channel (in the region of cooling and solidification of the melt) are convex toward the direction of motion of the plates. The curvature of these surfaces decreases with distance from the channel, i.e., the temperature levels off in the direction across the plates. The liquidus and solidus positions determine the width of the two-phase zone l_2 and the residence time of the melt in the two-phase state (time of solidification) $t_2 = l_2/(v \cos\chi)$, where χ is the angle between the velocity vector of the plates and the normal to the tangential line to the solidification isotherm. For the welding conditions considered, the mean values of these quantities over the z axis are $l_2 = 3.2 \cdot 10^{-4}$ m and $\bar{t}_2 = 4 \cdot 10^{-3}$ sec. Thus, the width of the transitional zone and the time of solidification have low values, which is caused by rather high temperature gradients and, correspondingly, by a high rate of cooling of the solidifying melt: $\bar{v}_T = (T_{l0} - T_e)/\bar{t}_2 = 12/(4 \cdot 10^{-3}) = 3 \cdot 10^3$ K/sec. For this reason, a fine crystalline structure is formed

in the crystallization region. To estimate the characteristic size of the dendrite cell d_1, we use the semi-empirical relation [13]: $d_1 = 1.13 \cdot 10^{-4} v_T^{-1/2} = 1.13 \cdot 10^{-4}/(3 \cdot 10^3)^{1/2} = 2.06 \cdot 10^{-6}$ m.

The height of the weld bed (see Fig. 3) formed in butt-welding in the region of the solidified metal is approximately 0.15–0.20 mm, which is consistent in the order of magnitude with the experimental data of [5].

Conclusions. A two-dimensional mathematical model of thermophysical processes that occur in laser butt-welding of plates made of a binary aluminum alloy with formation of a vapor channel has been developed. Based on this model, a computer code has been proposed for modeling thermophysical regimes of welding. This code allows determining the temperature fields in the article, the positions of the internal boundaries between the phases, the saturated vapor pressure in the channel, and the shape and depth of the vapor channel. The results of the numerical computations can be used to predict the size of zones occupied by different phases during the welding process and the degree of dispersion of the crystalline grains. For given laser power and plate thickness, the code also determines the optimal welding velocity that ensures formation of the liquid-phase region of a necessary volume without an end-to-end vapor channel (breakdown of the article by the laser beam).

This work was supported by the Russian Foundation for Basic Research (Grant Nos. 06-01-00080-r and 05-01-00311).

REFERENCES

1. N. N. Rykalin, A. A. Uglov, I. V. Zuev, et al., *Laser and Electron-Beam Processing of Materials* [in Russian], Mashinostroenie, Moscow (1985).
2. J. Kroos, U. Gratzke, and G. Simon, "Towards a self-consistent model of the keyhole in penetration laser beam welding," *J. Phys., D: Appl. Phys.*, **26**, 474–480 (1993).
3. V. A. Sudnik, D. Radai, and V. A. Dorofeev, "Computer modeling of laser-beam welding. Model and verification," *Svar. Proizv.*, No. 1, 28–33 (1997).
4. V. V. Semak, B. Damkroger, and S. Kempka, "Temporal evolution of the temperature field in the beam interaction zone during material processing," *J. Phys., D: Appl. Phys.*, **32**, 1819–1825 (1999).
5. É. A. Gladkov, A. I. Gavrilov, A. V. Maloletkov, et al., "Dynamic nonlinear model of the technological process of laser welding with deep melting," *Svar. Proizv.*, No. 12, 17–24 (2001).
6. V. S. Golubev, "Analysis of models of deep melting of metals by laser radiation," Preprint No. 83, Inst. Casting Problems, Russian Acad. of Sci., Shatura (1999).
7. V. T. Borisov, *Theory of the Two-Phase Zone of the Metal Ingot* [in Russian], Metallurgiya, Moscow (1987).
8. A. N. Oraevskii, "Gaussian beams and optical resonators," *Tr. Fiz. Inst. Lebedeva*, **187**, 3–59 (1988).
9. S. S. Kutateladze, *Fundamentals of Heat Transfer* [in Russian], Nauka, Novosibirsk (1970).
10. V. Semak and A. Matsunava, "The role of recoil pressure in energy balance during laser materials processing," *J. Phys., D: Appl. Phys.*, **30**, 2541–2552 (1997).
11. A. S. Basin and A. V. Shishkin, *Obtaining Silicon Plates for Solar Power Engineering: Methods and Technologies* [in Russian], Inst. Thermophys., Sib. Div., Russian Acad. of Sci., Novosibirsk (2000).
12. V. E. Zinov'ev, *Thermophysical Properties of Metals at High Temperatures: Handbook* [in Russian], Metallurgiya, Moscow (1989).
13. A. N. Cherepanov, "Analysis of similarity in processes of crystallization and structure formation of double alloys," *Metally*, No. 3, 69–76 (1988).